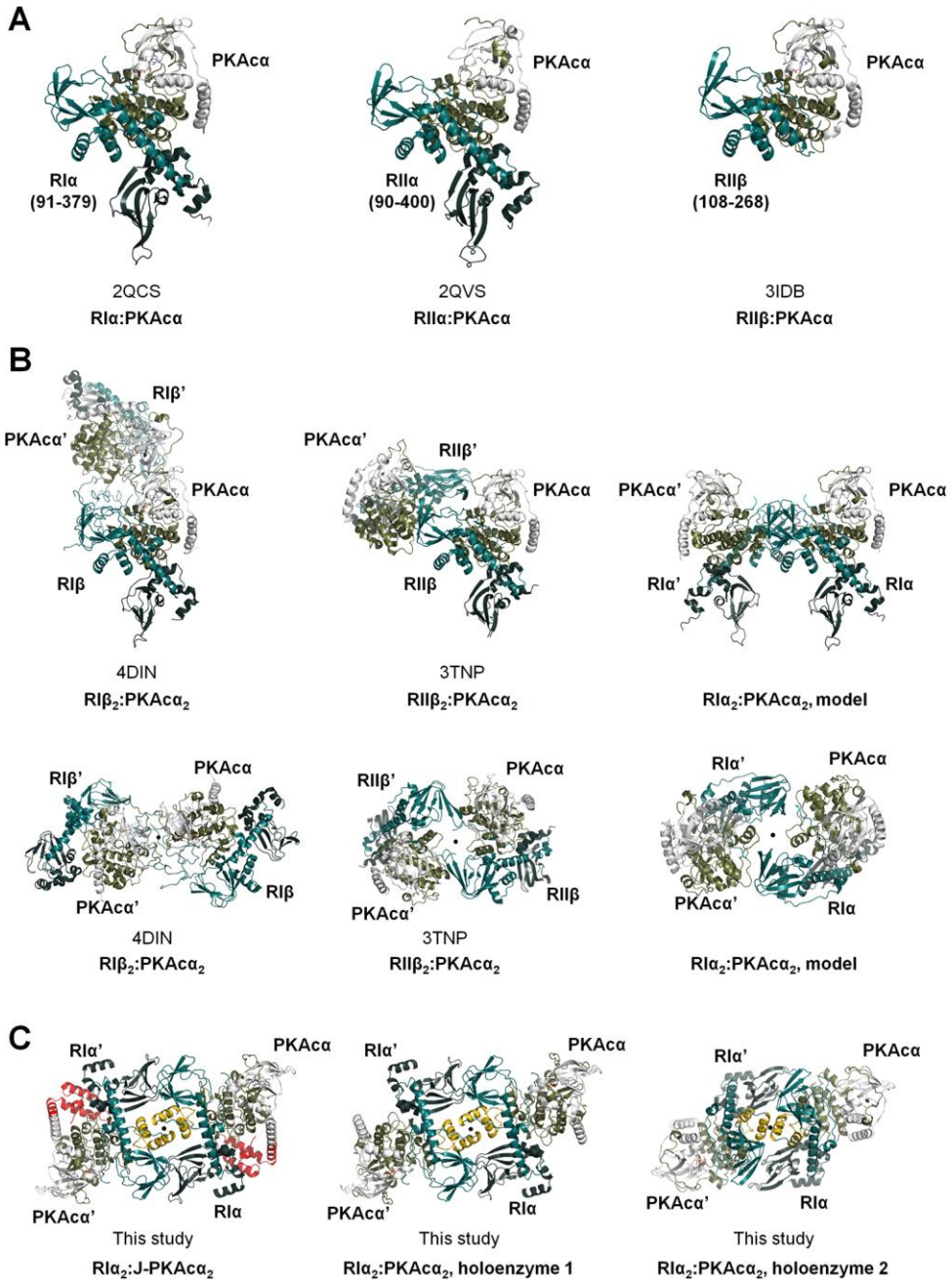


**Figure S1. Summary of structures of PKA R:PKAcα heterodimers and tetrameric PKA holoenzymes determined previously and in this study, Related to Figures 1, 4 and 5.**

(A) Previously reported structures of truncated PKA R:PKAcα heterodimers: RIα (91-379):PKAcα (PDB ID 2QCS, left) (Kim et al., 2007), RIIα (90-400):PKAcα (PDB ID 2QVS, middle) (Wu et al., 2007) and RIIβ (108-268):PKAcα (PDB ID 3IDB, right) (Brown et al.,

2009). (B) Previously determined wt $R_2$:PKAc$\alpha_2$ holoenzymes: RI$\beta_2$:PKAc$\alpha_2$ (PDB ID 4DIN, left) (Ilouz et al., 2012) and RII$\beta_2$:PKAc$\alpha_2$ (PDB ID 3TNP, midle) (Zhang et al., 2012) holoenzymes structures which were determined by X-ray crystallography, and the RI$\alpha_2$:PKAc$\alpha_2$ model based on crystal packing of two truncated RIα(73-244):PKAcα heterodimers (right) (Boettcher et al., 2011). On the top, the right R:PKAcα heterodimers are aligned at the same orientation; on the bottom the bird-eye view is shown for the three holoenzymes. (C) Bird-eye view of RI$\alpha_2$:J-PKAc$\alpha_2$ and RI$\alpha_2$:PKAc$\alpha_2$ tetrameric holoenzyme structures determined in this study. The twofold axis position for each holoenzyme is shown as a black dot in the middle.

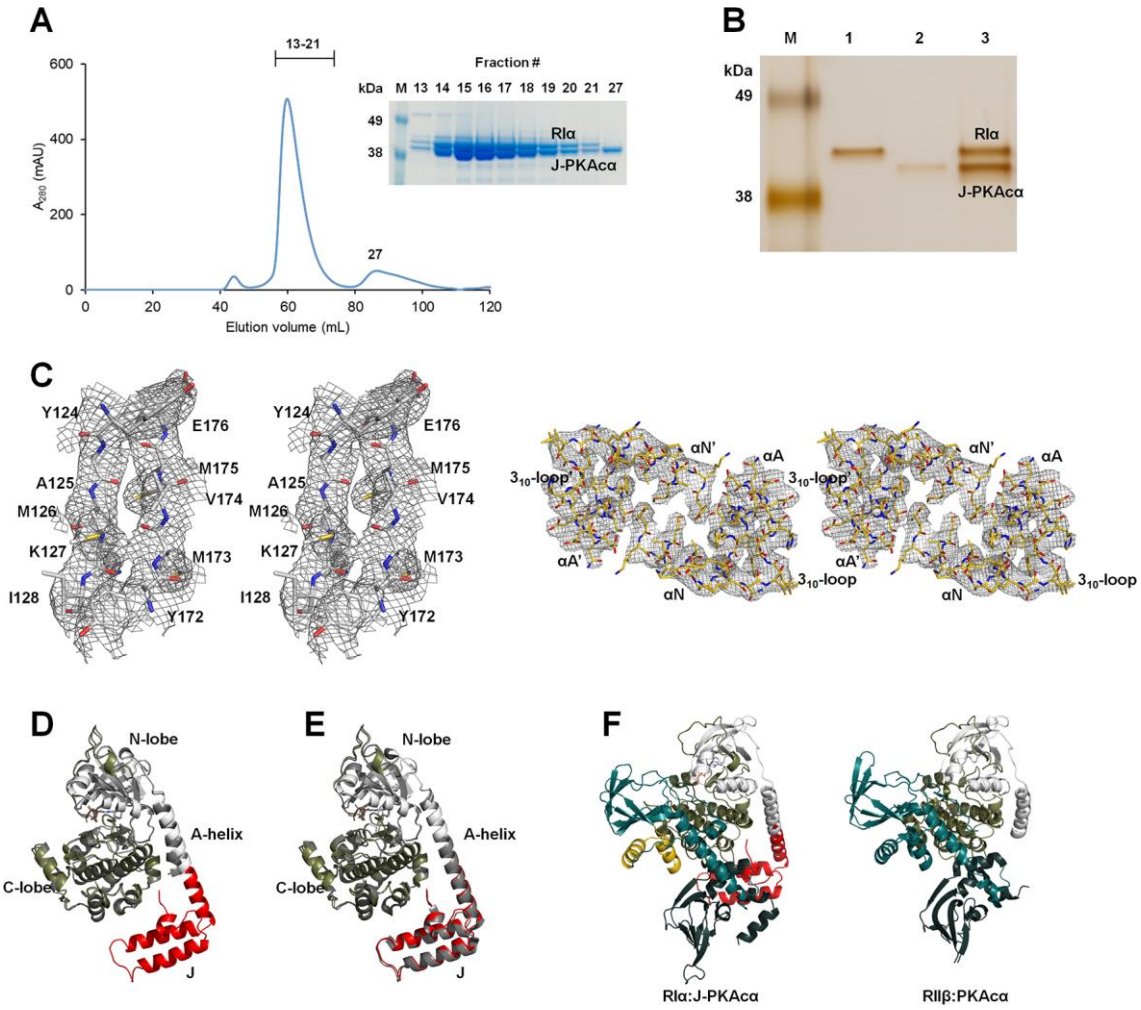


**Figure S2. Formation and structural analysis of the chimeric RIα$_2$:PKAcα$_2$ holoenzyme, Related to Figure 1.**

(A) Analytical gel filtration profile showing formation of RIα$_2$:J-PKAcα$_2$. (B) The diffracting crystals contain the full-length RIα$_2$:J-PKAcα$_2$ complex that was used for crystallization. The purified proteins RIα (lane 1), J-PKAcα (lane 2) and the dissolved diffracting crystals (lane 3) were run on a 7% tris-acetate SDS-PAGE gel and silver stained. (C) Cross-eyed stereo view of part of the RIα$_2$:J-PKAcα$_2$ holoenzyme structure (left) and the N3A-N3A' interface in the RIα$_2$:J-PKAcα$_2$ holoenzyme structure (right) in the 3.66 Å resolution 2Fo-Fc map at 1 σ. (D) Overlay of J-PKAcα (colored) in the chimeric holoenzyme and PKI-bound PKAcα (gray, PDB ID 1ATP).

(E) Overlay of J-PKAcα in the chimeric holoenzyme (colored) and PKI-bound J-PKAcα (gray, PDB ID 4WB7). (F) Side-by-side comparison of RIα:J-PKAcα in the chimeric holoenzyme and a canonical R:PKAcα heterodimer in the $RII\beta_2$:$PKAc\alpha_2$ holoenzyme (PDB ID 3TNP).

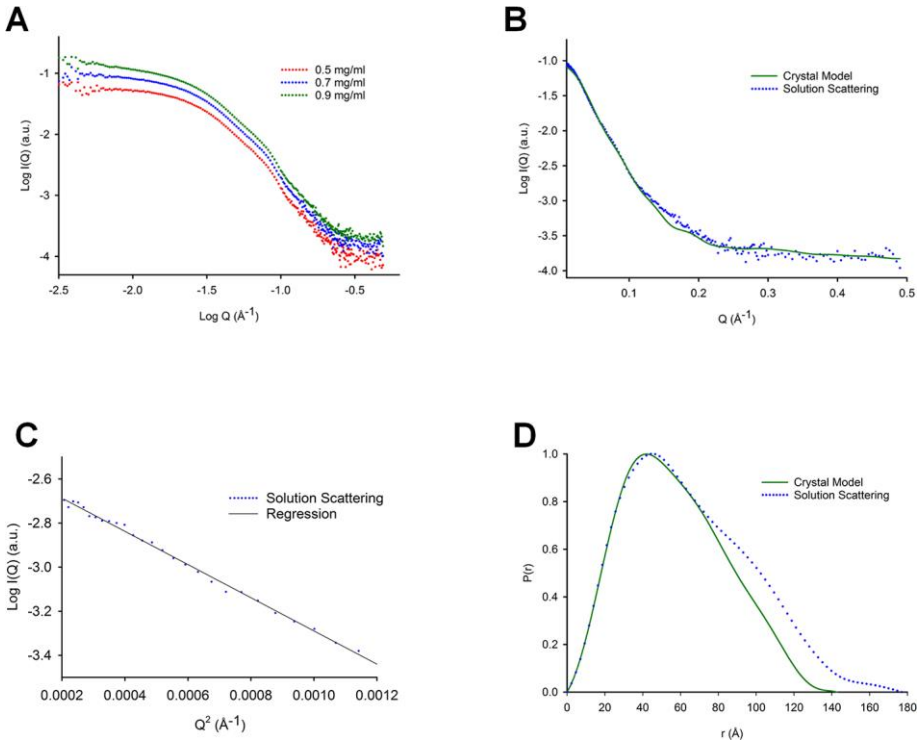


**Figure S3. SAXS results from RIα$_2$:J-PKAcα$_2$, Related to STAR methods.**

(A) SAXS profiles of RIα$_2$:J-PKAcα$_2$ at different concentrations. (B) Calculated scattering curve from crystal structure in continuous green line and SAXS experimental curve extrapolated to infinity dilution in blue dots. (C) Guinier plot, $I_0$: 0.081, $R_g$:48.8 ± 2.0 Å and $Q_{max}$*$R_g$: 1.26. (D) The P(r) functions from the crystal structure of RIα$_2$:J-PKAcα$_2$ in continuous solid green line and SAXS experimental data for the chimeric holoenzyme in blue dots.

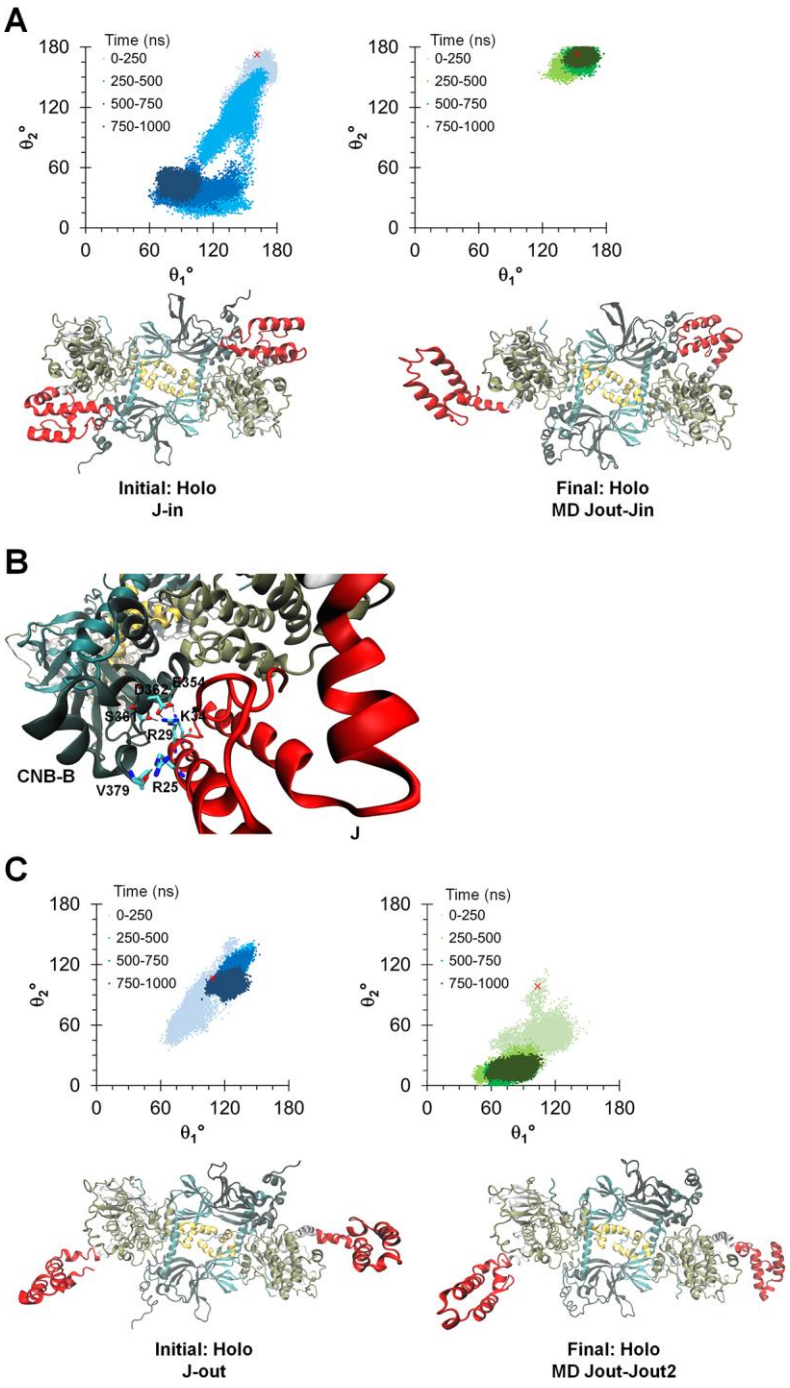


**Figure S4. The J-domain configurations during the MD simulations started from the J-in state model (A and B) and the J-out state model (C), Related to Figure 2.**

For each simulation of RIα$_2$:J-PKAcα$_2$, the top shows the orientation of the J-domain for each copy of the chimera in the holoenzyme, and the bottom shows the Initial (left) and final (right)

configurations of the J-domain in the holoenzyme. Hydrogen bonds that formed between the J-domain and CNB-B domain during the J-in state model simulation are shown in (B). The angles in both simulations are the same as those defined in Figure 2. The red ‘x’ indicates the initial conformation of the J-domain.

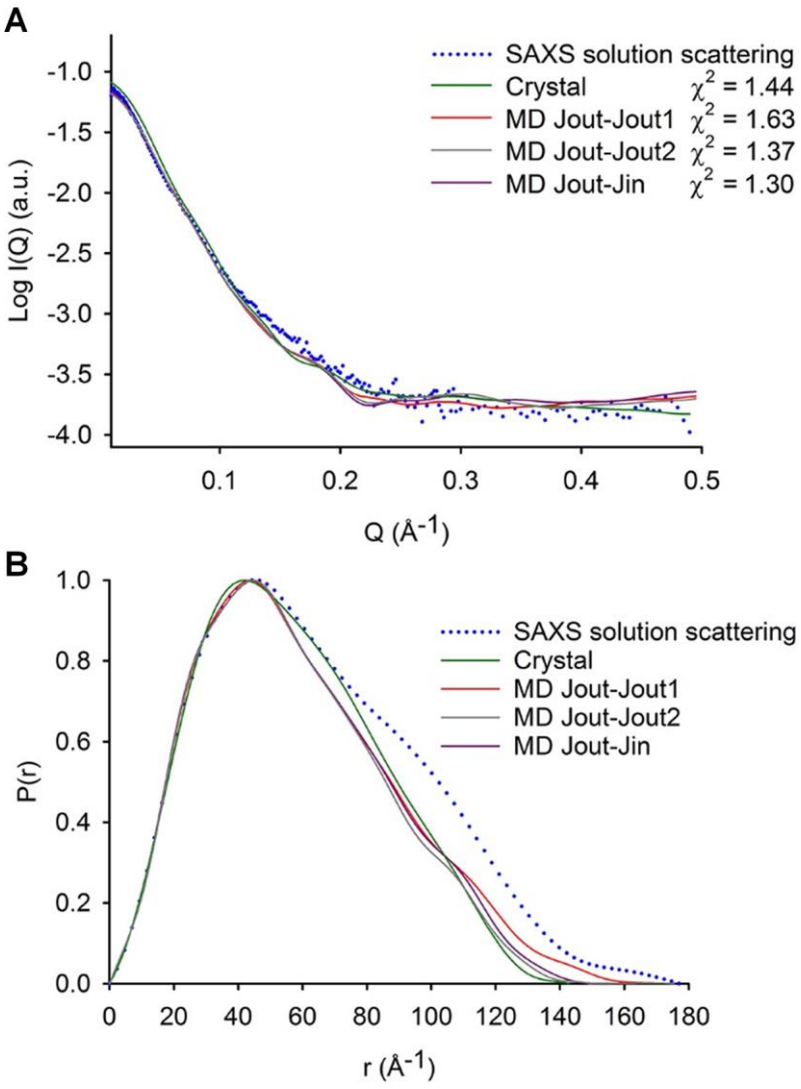


**Figure S5. Comparison among the final conformations from holoenzyme MD simulations, holoenzyme crystal and SAXS experimental curves, Related to STAR Methods.**

(A) Calculated scattering curves from holoenzyme crystal and final conformations of MD simulations in solid lines and SAXS experimental curve extrapolated to infinity dilution in blue dots. (B) The P(r) functions from MD final conformations and holoenzyme crystal in solid lines and SAXS experimental data for the chimeric holoenzyme in blue dots. Calculated $\chi^2$, $R_g$ and $D_{max}$ values are reported in Table S2.

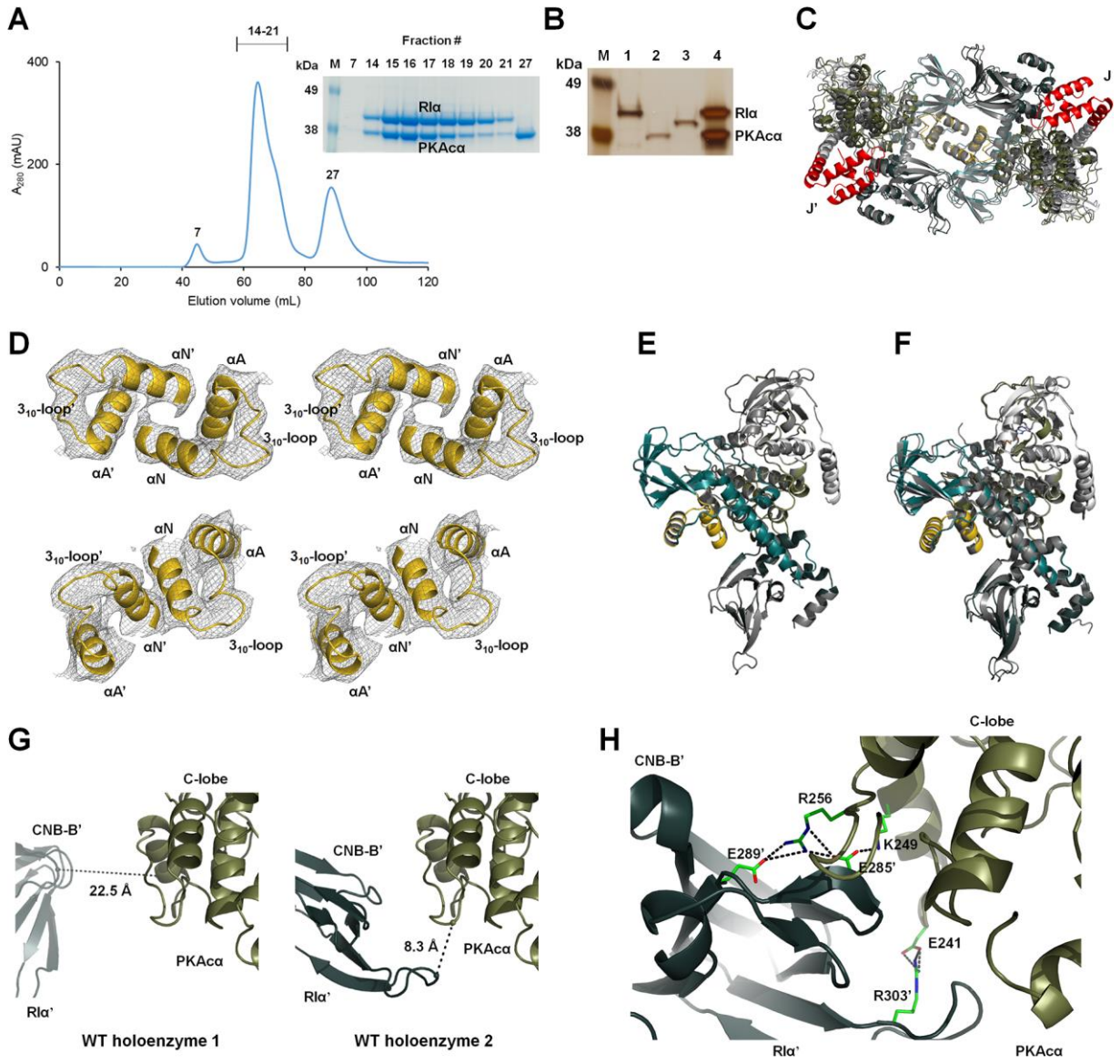


**Figure S6. Formation and structural analysis of the wt RIα$_2$:PKAcα$_2$ holoenzyme, Related to Figure 4.**

(A) Analytical gel filtration profile showing formation of RIα$_2$:PKAcα$_2$. (B) The diffracting crystals contain the full-length RIα$_2$:PKAcα$_2$ complex that was used for crystallization. The purified proteins RIα (lane 1), PKAcα (lane 2), J-PKAcα (lane 3) and the dissolved diffracting crystals (lane 4) were run on a 7% tris-acetate SDS-PAGE gel and silver stained. (C) Overlay of the RIα$_2$:PKAcα$_2$ holoenzyme 1 (gray) and chimeric RIα$_2$:J-PKAcα$_2$ holoenzyme (colored). (D)

Cross-eyed stereo view of the N3A-N3A' interfaces in the conformations 1 (top) and 2 (bottom) of the $RI\alpha_2$:$PKAc\alpha_2$ holoenzyme structure in the 4.75 Å resolution 2Fo-Fc map at 1 σ. (E) Overlay of the RIα:PKAcα heterodimers in the wt holoenzyme 1 (colored) and 2 (gray). (F) Overlay of RIα:PKAcα in the wt holoenzyme 1 (colored) and the previously reported RIα:PKAcα heterodimer (gray, PDB ID 2QCS). (G) The minimum Cα distances between PKAcα and RIα' in wt holoenzyme 1 (left) and 2 (right). (H) Formation of salt bridges between the C-lobe of PKAcα and the CNB-B' domain of RIα' in wt holoenzyme 2 during MD simulation.

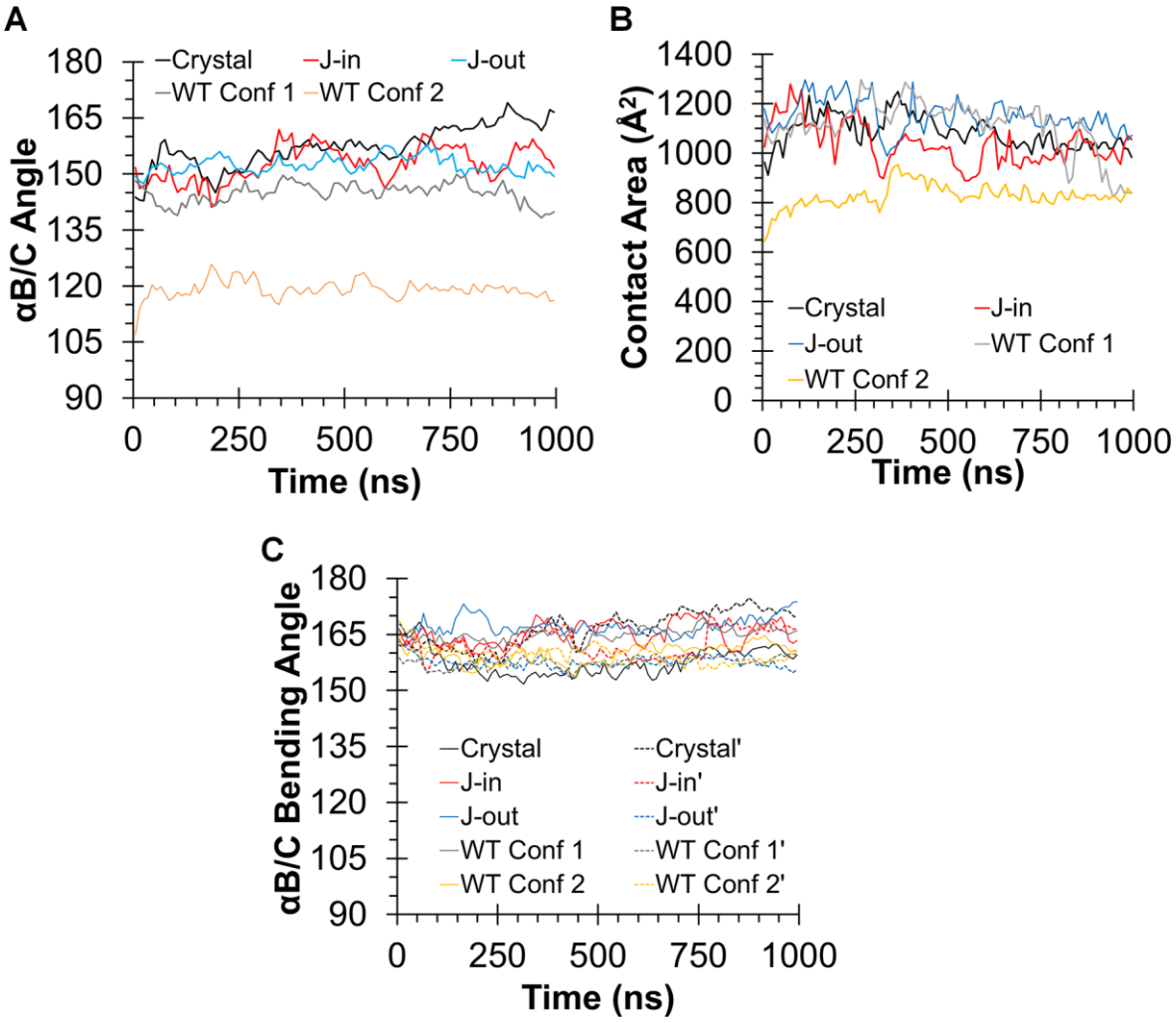


**Figure S7. The RIα-RIα' interfaces and dynamics of the αB/C-helix in the RIα chimeric holoenzyme (Crystal), models of the chimeric holoenzyme with both J-domains in J-in state (J-in) and with both J-domains in J-out state (J-out), and wt holo (WT) during MD simulations, Related to Figure 2.**

(A) Orientation between the two αB/C-helices in the RIα dimers as a function of time. (B) Contact area of the RIα-RIα' interfaces. (C) Linearity of the αB/C-helices as defined by the Cα atoms of D225-G235-K250. The αB/C-helices in simulations do not sample the bent conformation that is observed in the cAMP-bound RIα homodimer. Solid lines indicate the αB/C

bending angle in one R subunit while dashed lines indicate those in the symmetry-related R subunit in the holoenzyme.

**Table S1. Averaged B factors for the J-domain and the rest of J-PKAcα bound with RIα or PKI, Related to Figure 1.**

| | $B_J$[a] | $B_C$[b] | Ratio of $B_J$:$B_C$ |
|---|---|---|---|
| $RI\alpha_2$:J-$PKAc\alpha_2$ | 203.45 | 94.09 | 2.16:1 |
| J-PKAcα:PKI[c] | 63.54 | 34.39 | 1.85:1 |

[a] $B_J$: Averaged B factors of the J-domain (residues 1-69)
[b] $B_C$: Averaged B factors of the rest of J-PKAcα (residues 70-405)
[c] from PDB ID 4WB7 (Cheung et al., 2015)

**Table S2. SAXS structural parameters, Related to Figure 2.**

| Holoenzyme conformation | $R_g$ (Å) in reciprocal space | $R_g$ (Å) in real space | $D_{max}$ (Å) | $\chi^{2\,c}$ |
|---|---|---|---|---|
| SAXS solution scattering | 48.8 ± 2.0[d] | 50.0 ± 1.0 | 177 | N/A |
| Crystal[a] | 44.6 | 44.7 ± 0.5 | 142 | 1.44 |
| Jout-Jout1[b] | 44.6 | 44.6 ± 0.5 | 149 | 1.63 |
| Jout-Jout2[b] | 46.7 | 46.9 ± 0.7 | 176 | 1.30 |
| Jout-Jin[b] | 45.3 | 45.4 ± 0.5 | 151 | 1.37 |

[a] Calculated from the crystal structure

[b] Calculated from the final conformations of MD simulations

[c] Compared to experimental SAXS solution data

[d] Obtained from Guinier plot. The other Rg values were obtained from GNOM.

**Table S3. Thermal stability of the RIα$_2$:J-PKAcα$_2$ and RIα$_2$:PKAcα$_2$ holoenzymes, Related to Figure 4.**

| Tm[a] (°C) | - MgATP | + MgATP |
|---|---|---|
| RIα$_2$:PKAcα$_2$ | 52.93 ± 0.02 | 59.40 ± 0.03 |
| RIα$_2$:J-PKAcα$_2$ | 51.70 ± 0.01 | 58.90 ± 0.03 |
| ΔTm (wt/mutant) | 1.23 ± 0.02 | 0.50 ± 0.03 |

[a] Tm: temperature at which the protein denatures

All data are mean ± s.d. (n = 2 independent experiments).